

Article

# Coupling between Hydrodynamics and Chlorophyll *a* and Bacteria in a Temperate Estuary: A Box Model Approach

Élia Fernandes <sup>1,2,\*</sup>, Catarina Teixeira <sup>1,3</sup> and Adriano A. Bordalo <sup>1,3</sup> 

<sup>1</sup> Laboratory of Hydrobiology and Ecology, Institute of Biomedical Sciences (ICBAS), University of Porto, Rua Jorge Viterbo Ferreira, 228, 4050-313 Porto, Portugal; catarina@icbas.up.pt (C.T.); bordalo@icbas.up.pt (A.A.B.)

<sup>2</sup> School of Technology and Management, Polytechnic Institute of Viana do Castelo (ESTG-IPVC), Avenida do Atlântico, 4900-348 Viana do Castelo, Portugal

<sup>3</sup> Centre of Marine and Environmental Research (CIIMAR), Avenida General Norton de Matos, 4450-208 Matosinhos, Portugal

\* Correspondence: eliaf@estg.ipvc.pt; Tel.: +35-12-5881-9700

Received: 29 January 2019; Accepted: 18 March 2019; Published: 21 March 2019



**Abstract:** The spatial patterns of chlorophyll *a* and bacteria were assessed in a temperate Atlantic tidal estuary during seasonal surveys, as well as in consecutive summer spring and neap tides. A box model approach was used to better understand spatial and temporal dynamics of these key estuarine descriptors. The Lima estuary (NW Portugal) was divided into boxes controlled by salinity and freshwater discharge and balance equations were derived for each variable, enabling the calculation of horizontal and vertical fluxes of plankton and, therefore, production or consumption rates. Chlorophyll *a* tended to burst within the oligohaline zone, whereas higher counts of bacteria were found in the mesohaline stretch. Whenever the water column was stratified, similar tide-independent trends were found for chlorophyll *a* and bacterial fluxes, with net growth in the upper less saline boxes, and consumption beneath the halocline. In the non-stratified upper estuary, other controls emerged for chlorophyll *a* and bacteria, such as nitrogen and carbon inputs, respectively. The presented results show that, while tidal hydrodynamics influenced plankton variability, production/consumption rates resulted from the interaction of additional factors, namely estuarine geomorphological characteristics and nutrient inputs. In complex estuarine systems, the rather simple box model approach remains a useful tool in the task of understanding the coupling between hydrodynamics and the behavior of plankton, emerging as a contribution toward the management of estuarine systems.

**Keywords:** salinity; chlorophyll *a*; bacteria; hydrodynamics; box model; Lima estuary

## 1. Introduction

Estuaries all over the world are subject to increased pressure due the alterations in the land uses and increase of the population [1]. These alterations result in an accretion of inorganic and organic compounds, microbial loads, and changes in the discharge patterns of freshwater in the estuarine and marine coastal environments, resulting in complex ecosystem behaviors [2]. Estuaries are influenced by both marine and riverine characteristics, and their features depend of tidal pulses, freshwater flow, hydrodynamic, and autochthonous biological processes [3]. Mesotidal temperate estuaries are characterized to have semi-diurnal tidal cycles in the range of 2–4 m. Every fortnight, the influence of the moon generates another tidal event called spring tide, characterized by increased tidal amplitude. The complexity of estuarine circulation system may be described through a combination of several components, such as tidal forcing, depth and width, freshwater flow, as well as meteorological

forcing [4]. The complex interaction between all the different processes and the need to quantify these interactions led to the development of models capable of evaluating various properties in space and time. In the case of a box model, the complex estuarine circulation system is simplified, being reduced to boxes (or reservoirs) linked by fluxes, and it is assumed that the boxes have homogeneous content. However, the concentration of a given descriptor in the box can vary as a function of time, due to input to (or loss of) the box, or due to production, consumption, or decrease of that descriptor within the box. Vertically-stratified estuaries add an important level of complexity to the modelling analysis. In an estuary, partially mixed or strongly stratified, the basic net circulation consists of an upper layer transporting a mass of fresh or brackish water toward the sea, and a lower layer moving in the opposite direction [5]. This movement of saltier water mass results in a net vertical flow, with upward direction and amplitude determined by the intensity of mixing in the river [6]. Pritchard [7] developed a relatively simple model that can predict concentration distributions along the length of an estuary, in both upper and lower layer, based on various simplifying assumptions, such as, steady-state conditions, conservative pollutant behavior, and uniform constituent concentration within each layer or each segment. The model estimates the vertical non-advective exchange coefficients for each box, which are used to establish balance equations for the studied variable, allowing the calculation of horizontal and vertical fluxes, as well as the respective rates in order to ascertain its production or consumption [4]. The box model uses the property of salinity as a conservative tracer [8], in order to calculate the required transfer coefficients. Thus, as the water circulation controls the physical distribution of dissolved and particulate matter, the abundance in each box can be used to calculate the flux and, simultaneously, sources and sinks, i.e., a non-conservative fluxes (e.g., chlorophyll *a* and bacteria), along the salinity gradient. This way, some light can be shed on the behavior patterns of these quantities within the estuarine boundaries.

The metabolic balance of an estuarine system is dependent on the primary production and community respiration. The primary production depends on physical (light availability, temperature), chemical (nutrients), and biological (phytoplankton biomass, species composition, size and structure, grazing) factors (e.g., [9–11]). The freshwater inflow may have a tremendous effect since it controls residence time, and the susceptibility of the ecosystems to algal blooms, with effects on the food web [12]. Tides also influence phytoplankton dynamics leading to a biomass increase during neap tides, and a decrease during spring tides [9,13], and gradient variations in the ebb and flood tides [14]. As the phytoplankton rapidly responds to changes in the environmental conditions, the dynamic structure of phytoplankton communities reflects the health of the aquatic ecosystems [15,16].

Bacteria also have a key role on the functioning of estuaries, since the community is crucial for the biogeochemical cycle of nutrients [17,18] and the turnover of organic matter [19]. In some estuaries, bacteria tend to reach a state of trophodynamic equilibrium [20] and, therefore, the normal behavior of those quantities differ from the conservative pattern, i.e., numbers do not decrease linearly with an increase of salinity [21].

The aim of this study was to understand the spatial dynamics of chlorophyll *a* and bacteria along a temperate estuary during the ebb tide at different flow/seasonal regimes by means of a box model approach. The different regimes were assessed through seasonal neap surveys, in order to cover different runoff conditions. Furthermore, an additional spring tide survey was carried out during the summer, thus covering two different tidal regimes (neap and spring). This approach led to a better understanding of the spatial and temporal dynamics of plankton through modeling, contributing to improving the knowledge of the dynamics and transformation processes within the estuary, emerging as a valuable tool for managers.

## 2. Materials and Methods

### 2.1. The Study Area

The Lima estuary is located in NW Portugal (41.68° N, 8.84° W) (WGS84), and belongs to the Portuguese hydrographic region of the Minho and Lima (RH 1), according to the Water Framework Directive [22] (Figure 1). The estuary extends over 20 km covering an area of 10.4 km<sup>2</sup>, and has a semidiurnal, mesotidal regime (0.2–3.9 m) [23]. According to the morphology, bathymetry, salinity, and the presence/absence of saltmarshes, the estuary can be divided into three geomorphological zones: lower, middle, and upper estuary (Figure 1).

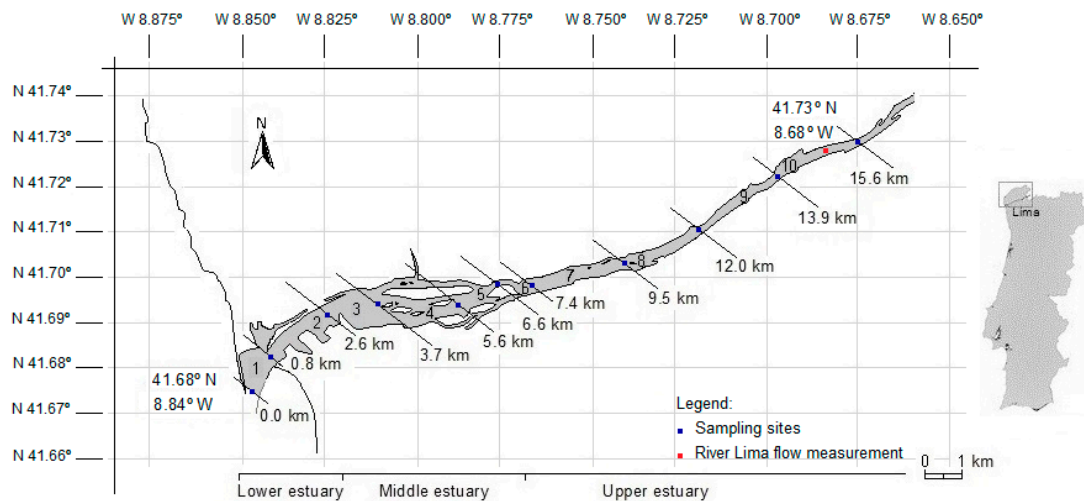


**Figure 1.** Map of the Lima estuary, sampling locations, and box boundaries used in the model.

The first zone, located within the first 2.5 km, is a navigation channel with walled banks, being narrow and deep (9 m), and characterized by the presence of seawater. The area is rather industrialized, with anthropogenic modifications such as the presence of a jetty at the river mouth deflecting the flow to the south, constant dredging operations, large shipyard, a commercial sea-port, a marina, and a fishing harbor [24]. The middle estuary encompasses an area of saltmarshes with several sandy islands, and intertidal channels. Further upstream, the estuary continues as a narrow and shallow channel (0.5–1 m deep), remaining in a natural state with intertidal areas and undisturbed banks. This zone is characterized by low salinity water (oligohaline and freshwater), and is affected by agricultural run-off, domestic, and industrial wastewater discharges leading to the accretion of nutrients and other substances transported from urban, industrial, and agricultural areas into the estuary [25].

### 2.2. Sampling

Seasonal surveys were carried out on the ebb of four neap tides (25 February 2014; 2 June 2014; 1 September 2014; and 11 November 2014), and on the ebb of a spring tide (10 September 2014). Each survey started 1:30 h before low tide slack water and lasted ca. 2:30 h to reduce the error due to the tide impact. In addition, sampling was performed from downstream (estuary mouth) to upstream (river), in order to follow the tide excursion, thus minimizing the hourly impact of the tide. Samples were collected from 11 locations along 15.6 km, corresponding to the navigable portions of the estuary, corresponding to 10 boxes (Figure 1). The boundaries for the boxes were chosen having into account geomorphological, geographic, and hydrological aspects of the Lima estuary. Particular attention was given to the sediment type (lower and middle estuary), the presence of saltmarshes, sandy islands, and intertidal channels (middle estuary), and the presence of population clusters and/or constructed structures (lower, middle, and upper estuary). The smaller size of downstream boxes result from the presence of stronger vertical and longitudinal salinity gradient. Vertical profiles of salinity and

temperature were obtained with a YSI 6920 CTD multiprobe, calibrated according to the instructions from the manufacturer. The data required for vertical profiles of chlorophyll *a* and bacteria, as well as for the physical-chemical characterization were achieved from the analytical determination in samples collected from the water column with a Van Dorn bottle (surface, middle water, and near bottom). The collected samples were kept refrigerated in an ice chest, transported to the laboratory, and processed within 8 h.

### 2.3. Analytical Procedures

For chlorophyll *a* determinations, 500 mL of water were filtered onto cellulose acetate 0.45  $\mu\text{m}$  membranes (HA Millipore). Chlorophyll *a* was analytically determined by molecular absorption spectrophotometry after extraction using 90% acetone [26] using the SCOR-UNESCO equations [27]. For total count of bacterial cells, water samples were fixed with formaldehyde (4% v/v). Subsamples (3 mL) were stained with 4',6'-diamidino-2-phenylindole (DAPI), and filtered onto black 0.2  $\mu\text{m}$  Nucleopore polycarbonate membranes (Whatman, Little Chalfont, Buckinghamshire, UK) [28]. The bacterial cells were counted directly with an epifluorescence microscope (Labphot, Nikon, Tokyo, Japan) equipped with a 100 W high-pressure mercury lamp and a specific filter sets (UV-2B), at  $1875\times$  magnification. A total of 20 random microscope fields in different parts of the filter were counted in order to accumulate at least 300 cells per filter.

### 2.4. River Flow

The river flow data were generated from weekly measurements carried out between January 2014 and February 2015, in the upper estuary ( $41.72^\circ$  N,  $8.68^\circ$  W) (Figure 1). The velocity-area method was used [29]. The stream cross-section was divided into numerous vertical subsections. In each subsection, the area was obtained by measuring its width and depth. The sum of areas yielded the cross-section of the river. The velocity was then measured using weighted floats (five to ten replicates), i.e., the velocity was equal to the distance between the cross-sections (bridge—11.5 m) divided by the time taken by the float to cover this distance. The flow of the river was computed by multiplying the cross-section area of the river by the measured velocity.

### 2.5. The Box Model

From previous studies, it was found that, during summer, the Lima estuary tends to be vertically stratified to partially mixed in the lower and middle stretches, respectively (data not shown). Further upstream the estuary was found to be always vertically homogeneous in terms of salinity. A model with 10 boxes was adopted for this study, with two layered boxes in the first downstream sections, being the A-upper for the surface layer and B-lower for the deeper layer, and one-layer in the remaining boxes. The salinity used to define the stratification of the estuary water column, (i.e., the boundary between the upper and lower layers of the box) was 18 ppt corresponding to meso-polyhaline classification (see below). In the most upstream vertically stratified box, freshwater flowed downstream on the top layer, while in the bottom layer there was no movement of salt water to upstream. As such, it was assumed the existence of vertical advective and non-advective fluxes between the two layers, and that diffuse longitudinal (non-advective) processes between the boxes were insignificant being, therefore, the contents of each box remains homogeneous longitudinally. The layout of the two layer boxes is presented in Figure 2B.  $Q_1$  represents the flow rate ( $\text{m}^3 \text{s}^{-1}$ ) of the water with salinity  $S_1$ , out of the layer through the downstream boundary of the box;  $Q_2$  is the flow rate ( $\text{m}^3 \text{s}^{-1}$ ) of water into the top layer with salinity  $S_2$  through the upstream boundary;  $S_1$  and  $S_2$  are the mean salinities of the upper layer at the two box boundaries. Likewise,  $Q_3$  represents the flow rate ( $\text{m}^3 \text{s}^{-1}$ ) of water with salinity  $S_3$  into the box;  $Q_4$  is the flow rate out ( $\text{m}^3 \text{s}^{-1}$ ) of the box of water with salinity  $S_4$ ;  $S_3$  and  $S_4$  are the mean salinities of the lower layer at the two box boundaries. The non-advective (diffusive) vertical exchange coefficient between the two layers is represented by the letter  $E$ .  $S_U$  and  $S_L$  represent the mean salinities of the A-upper and B-lower layers, respectively.

$Q_V$  is the vertical flow rate ( $\text{m}^3 \text{s}^{-1}$ ) of water from the lower layer into the upper layer with salinity  $S_V$ , being  $S_V$  the average of the salinities  $S_U$  and  $S_L$  (Equation (1)):

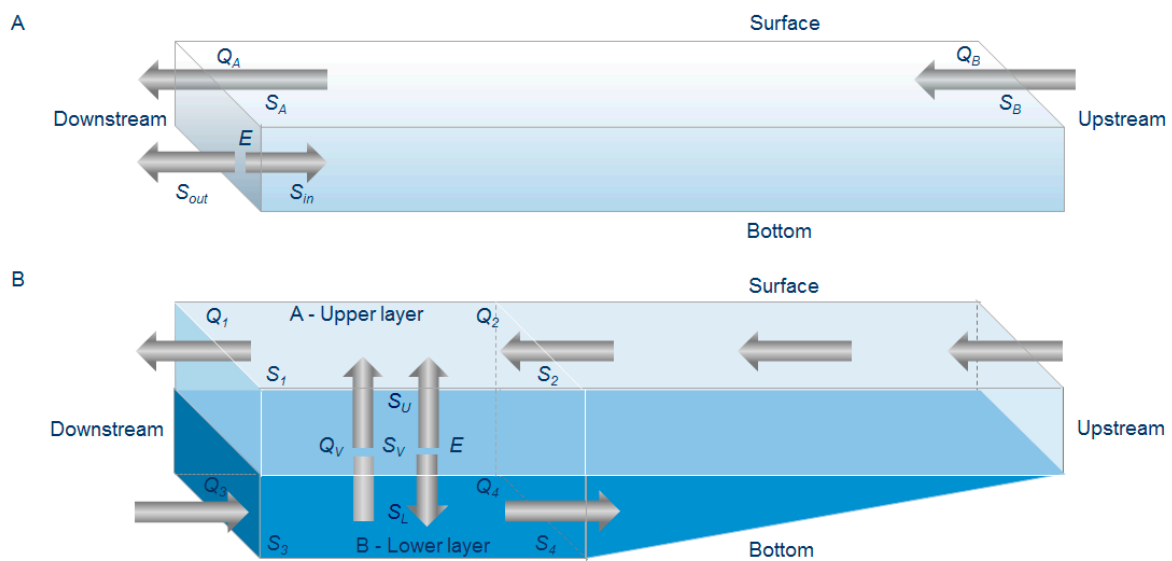


**Figure 2.** Layout of the box model used in this study: fluxes and exchange coefficients for the one layer box model (A), and two-layer box model (B).  $Q_x$  represents the flow rate ( $\text{m}^3 \text{s}^{-1}$ ) of the water with salinity  $S_x$ .  $E_v$  represents the non-advective vertical exchange coefficient between the two layers.  $S_U$ ,  $S_L$  and  $S_V$  represents mean salinities.  $E$  corresponds to the non-advective exchange coefficient.

$$S_V = \frac{(S_U + S_L)}{2} \tag{1}$$

Assuming the existence of steady state conditions and according to Figure 2B, the following salt equations conservation equations, could be obtained for the upper and lower layer, respectively, as described by Bordalo and Vieira [4]:

$$\text{Upper layer } Q_2 S_2 + Q_V S_V + E(S_L - S_U) = Q_1 S_1 \tag{2}$$

$$\text{Lower layer } Q_4 S_4 + Q_V S_V + E(S_L - S_U) = Q_3 S_3 \tag{3}$$

and, as result of the water mass balance:

$$Q_V = Q_1 - Q_2 = Q_3 - Q_4 \tag{4}$$

The calculation started at the most upstream box with two layers. In this box, the freshwater flux in the upper layer toward ocean ( $Q_2$ ) equals the river discharge, with no flow toward upstream, resulting in a  $Q_4$  equal to 0. Since river discharge and salinity data were known, it was possible to calculate  $Q_1$  and  $Q_3$  [4]. Then, the calculations were repeated (Equations (2)–(4)) for the adjacent boxes consecutively toward the mouth of the estuary. Among the calculated values, those obtained for the exchange coefficients were essential to define the sources and sinks of both plankton parameters under study (chlorophyll  $a$  in  $\text{mg m}^{-3}$ ; bacteria in  $\text{cells mL}^{-1}$ ). To obtain the balance equations for each variable, salinity was replaced by the corresponding concentration values. The resulting balance equations for the A-upper and B-lower layers were, respectively:

$$\text{Upper layer } C_2 Q_2 + Q_V \left( \frac{C_U + C_L}{2} \right) + E(C_L - C_U) - Q_1 C_1 = P_U \tag{5}$$

$$\text{Lower layer } C_3 Q_3 - Q_V \left( \frac{C_U + C_L}{2} \right) - E(C_L - C_U) - Q_4 C_4 = P_L \tag{6}$$

$P_U$  and  $P_L$  were the concentration fluxes into or out of the upper and lower layers of the box, respectively (in  $\text{mg s}^{-1}$ ,  $\text{cells s}^{-1}$ ). These values indicated the gain (+) or loss (−) of a quantity, therefore, the presence of a net source or sink (i.e., non-conservative flux). The results obtained of  $P_U$  and  $P_L$  were divided by the respective layer volume, this procedure being necessary because the layers of each box had different volumes. The objective of this calculation was to obtain the rates of production or loss of chlorophyll *a* ( $\text{mg m}^{-3} \text{s}^{-1}$ ), and bacteria ( $\text{cells m}^{-3} \text{s}^{-1}$ ).

For the remaining one-layer boxes, freshwater flow entering and leaving the box was represented by  $Q_B$  ( $\text{m}^3 \text{s}^{-1}$ ) and  $Q_A$  ( $\text{m}^3 \text{s}^{-1}$ ; Figure 2A), with salinity  $S_B$  and  $S_A$ , respectively.  $E$  corresponded to the non-advective (diffusive) horizontal exchange coefficient between adjacent boxes, and  $S_{in}$  and  $S_{out}$  the salinities inside and outside the box, being the equations for salt conservation and water mass balance:

$$Q_B S_B + E(S_{out} - S_{in}) = Q_A S_A \quad (7)$$

$$Q_B = Q_A \quad (8)$$

After the calculation of the exchange coefficients, the concentration flux of the studied variables into or out of the box ( $P$ ;  $\text{mg s}^{-1}$  or  $\text{cells s}^{-1}$ ) were obtained by replacing the salinity by its concentration (Equation (9)). The concentration flux was then divided by the box volume:

$$Q_B(C_B - C_A) + E(C_{out} - C_{in}) = P \quad (9)$$

For the box model, the obtained salinity values at each sampling site were used to classify water masses according to the Venice System [30] and the Water Framework Directive [31], i.e., freshwater (salinity < 0.5), brackish water (0.5–30), and seawater or euhaline water (>30), with brackish water subdivided into three groups, oligohaline (0.5–5), mesohaline (5–18), and polyhaline (18–30).

## 2.6. Data Analysis

The generation time was calculated with the values obtained from the box model for the bacterial fluxes ( $\text{cells m}^{-3} \text{h}^{-1}$ ), and the total cells counts ( $\text{cells m}^{-3}$ ), whenever a positive bacterial flux was found, according to Robarts et al. [32]

Vertical map profiles of salinity, chlorophyll *a* concentration and bacterial cells number along the main estuarine axis were created using Surfer 8.01 software (Golden Software Inc, Boulder, CO, USA), using kriging (linear variogram model) as the gridding method. *T*-tests were conducted to compare every two surveys, with a minimum  $n = 21$  and a maximum  $n = 28$ . ANOVA was performed on the entire seasonal set, and also for the dataset from neap and spring summer tides. Statistical tests were performed using the STATISTICA 13.0<sup>®</sup> software package.

## 3. Results

### 3.1. Bacteria and Chlorophyll *a* Profiles

The salinity profiles for the February and November surveys showed a well-mixed estuary in most of its extent, with polyhaline water confined to the first 2 km (Figure 3), owing to the inherent river discharge in winter and the fall ( $>192 \text{ m}^3 \text{ s}^{-1}$ ). The remaining surveys contours showed that a salt wedge (salinity above 30) introduced during the flood tide, remained within the estuary during low slack ebb tide. For June and September surveys, the salt wedge was located in the middle estuary around 3.5–4 km and 4–4.5 km, respectively. Nevertheless, the position of the boundary for 18 salinity was very similar for these surveys (4.5–5 km). The freshwater boundary reached km 3.5–4.5 during February and November, while not exceeding km 12 during June and September (Figure 3). Brackish water represented the largest water mass for winter and fall seasons and freshwater for the remaining ones.

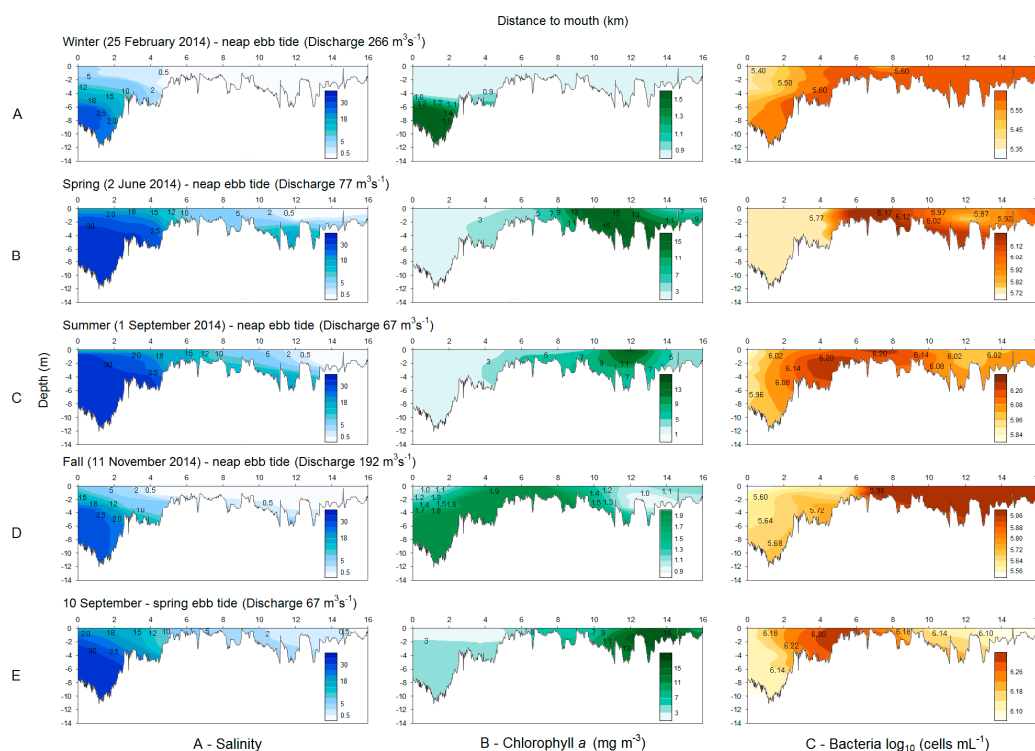


**Figure 3.** Longitudinal profile of salinity, chlorophyll *a* ( $\text{mg m}^{-3}$ ), and bacteria ( $\log_{10}$  cells  $\text{mL}^{-1}$ ) during seasonal neap tide (A–D) and the spring tide (E) surveys.

Comparing neap and spring tides, the longitudinal salinity profiles showed that the salt wedge was located about 4–4.5 km from the river mouth during neap tide, while during the spring tide survey it moved downstream to 2–2.5 km (Figure 3C,E). Inversely, the freshwater limit was found at 12–13 km upstream the river mouth in the neap survey, and pushed further upstream to 14.5–15.5 km during spring tide, being the discharge rate similar. The oligohaline water mass had an extension of ca. 7.5 km in the spring tide survey, but decreased to 2 km in the neap survey (Figure 3C,E).

The overall concentration of chlorophyll *a* in the estuary was significantly different for the different seasonal surveys ( $t$ -test  $p < 0.05$ ), with the exception of summer and spring surveys ( $t$ -test  $p > 0.05$ ). Chlorophyll *a* bloomed in spring and summer ( $15.69$  and  $16.50 \text{ mg m}^{-3}$ , respectively) in the upper low salinity stretches of the estuary (Figure 3), being the lowest value recorded in the winter survey ( $0.57 \text{ mg m}^{-3}$ ) (Table 1).

**Table 1.** Concentration ranges of chlorophyll *a* and bacteria in the Lima estuary.

Season	Concentration Range	Salt Water Stretch				
		Freshwater	Oligohaline	Mesohaline	Polyhaline	Seawater
Winter	Chlorophyll <i>a</i> ( $\text{mg m}^{-3}$ )	0.57–0.75	0.57–1.00	0.66–0.91	1.58	-
	Bacteria ( $\log_{10}$ cells $\text{mL}^{-1}$ )	5.50–5.68	5.38–5.66	5.40	5.55	-
Spring	Chlorophyll <i>a</i> ( $\text{mg m}^{-3}$ )	4.90–14.30	15.24–15.69	1.50–6.20	1.13–3.95	1.14–3.83
	Bacteria ( $\log_{10}$ cells $\text{mL}^{-1}$ )	5.77–6.06	6.04–6.05	5.53–6.23	5.55–5.81	5.52–5.78
Summer	Chlorophyll <i>a</i> ( $\text{mg m}^{-3}$ )	3.88–5.30	11.95–16.50	3.37–6.93	1.05–2.72	0.96–2.92
	Bacteria ( $\log_{10}$ cells $\text{mL}^{-1}$ )	5.99–6.08	5.98	6.02–6.26	5.95–6.24	5.78–6.21
Fall	Chlorophyll <i>a</i> ( $\text{mg m}^{-3}$ )	0.96–2.72	1.22–2.27	0.96–1.67	1.30–1.92	-
	Bacteria ( $\log_{10}$ cells $\text{mL}^{-1}$ )	5.63–6.00	5.57–5.69	5.53–5.73	5.62	-
Summer (spring tide)	Chlorophyll <i>a</i> ( $\text{mg m}^{-3}$ )	9.78	7.13–17.04	1.86–7.02	1.50–4.16	3.37–4.87
	Bacteria ( $\log_{10}$ cells $\text{mL}^{-1}$ )	6.06	6.09–6.16	6.23–6.35	6.08–6.26	6.07–6.13

For the summer neap and spring tidal surveys, the overall concentration of chlorophyll *a* in the estuary was not significantly different between the two tides ( $t$ -test  $p > 0.05$ ). The spatial variation was also similar, with chlorophyll *a* increasing toward upstream, reaching the highest concentrations ( $\sim 17.0 \text{ mg m}^{-3}$ ) within the upper estuary (Figure 3C,E). The lowest values were found during neap tide in seawater ( $0.96$ – $2.92 \text{ mg m}^{-3}$ ), i.e., the lower estuary (Table 1).

Regardless of the tide and season, chlorophyll *a* biomass always peaked in the 0.5–5 oligohaline stretch of the estuary (Table 1 and Figure 4). During the summer neap tide survey, chlorophyll *a* decreased progressively from 6.96–0.96 mg m<sup>-3</sup>, in the 5–35 salinity range, and salinity explained 61% ( $p < 0.0001$ ) of the chlorophyll *a* variability. In the summer spring tide survey, the concentration of chlorophyll *a* decreased in the salinity range 0–16, varying from 17.04–1.86 mg m<sup>-3</sup>, increasing again (up to 4 mg m<sup>-3</sup>) in higher salinities denoting the possible influence of the marine environment (Figure 4C). The observed patterns suggest the presence of other processes besides dilution, with a chlorophyll *a* sink at the mesohaline range.

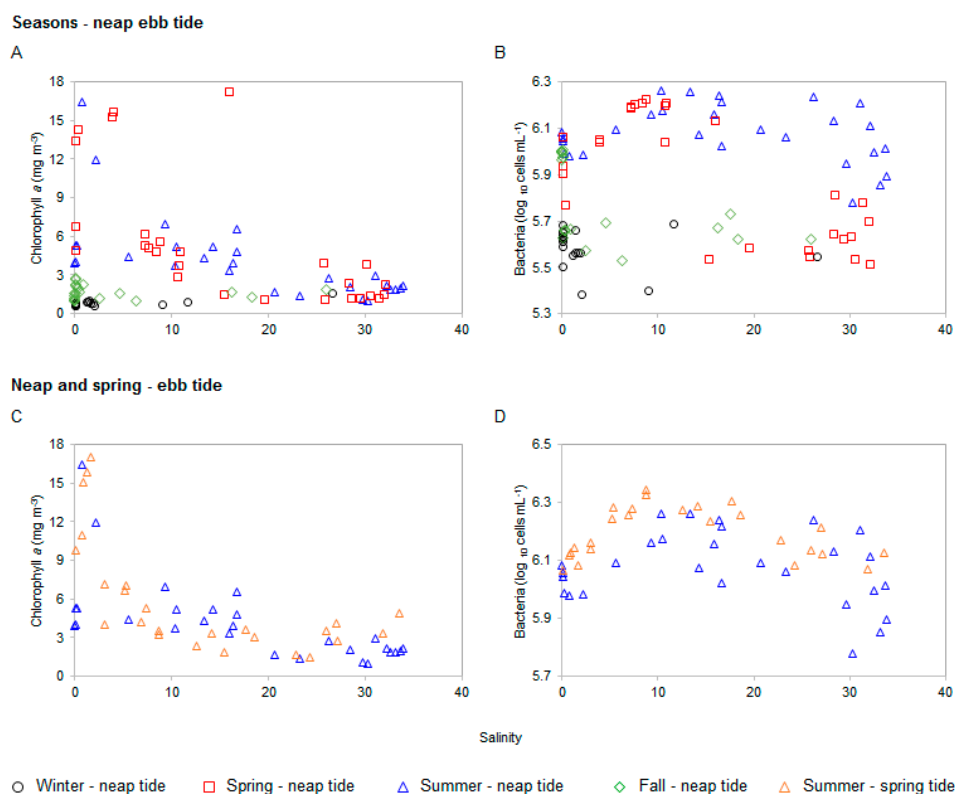


**Figure 4.** Relationship between chlorophyll *a*, and bacteria versus the conservative tracer salinity for seasonal neap tides (A,B), and a summer neap and spring tides (C,D) in the Lima estuary.

Bacteria presented a clear seasonal behavior. During the warmest period of the year, the highest concentrations were found in the middle estuary, within the mesohaline stretch, downstream the chlorophyll *a* maxima ( $1.7\text{--}1.8 \times 10^6$  cells mL<sup>-1</sup>, respectively during spring and summer). In both surveys, bacteria tended to increase from freshwater to the mesohaline interval (salinity 18), then decreased toward seawater (Figure 4B), suggesting the existence of different bacterial communities for each stretch of the estuary. In the remaining surveys, higher bacterial numbers were found in freshwater ( $4.8 \times 10^5$  cells mL<sup>-1</sup> for the winter survey, and  $1.0 \times 10^6$  cells mL<sup>-1</sup> for the fall survey (Figure 4B). Winter survey presented decreased bacterial abundance ( $t$ -test  $p < 0.0001$ ), independently of the salinity range, with the lowest value being found in seawater by the mouth of the estuary ( $0.25 \times 10^6$  cells mL<sup>-1</sup>).

Similar bacterial longitudinal distribution profiles were observed between neap and spring tides summer surveys (Figures 3 and 4). The highest concentrations were always found in the middle estuary ( $2.2 \times 10^6$  cells mL<sup>-1</sup> during the spring tide). At the seawater end-member, the values were always below  $1.6 \times 10^6$  cells mL<sup>-1</sup>, and in the freshwater end-member below  $1.2 \times 10^6$  cells mL<sup>-1</sup>. It was found that when tides were compared, the spring tide fostered higher bacterial abundance ( $t$ -test  $p < 0.0005$ ). Regardless of the tide, bacteria tended to increase in the salinity range 8–15 (neap tide), and 9–12 (spring tide), further decreasing in a monotonically fashion toward seawater (Figure 4). Again, this behavior suggested the existence of different bacteria communities adapted to each stretch of estuary with salinity ca. 10 acting as a threshold.

Information on additional environmental variables measured during the seasonal surveys can be found as supplementary material (Tables S1–S3, Figure S1).

### 3.2. Box Model

The river flows measured for the Lima estuary were  $266 \text{ m}^3 \text{ s}^{-1}$  (winter),  $77 \text{ m}^3 \text{ s}^{-1}$  (spring),  $67 \text{ m}^3 \text{ s}^{-1}$  (summer), and  $192 \text{ m}^3 \text{ s}^{-1}$  (fall), and were used to feed the box model. Vertical salinity stratification, with an upper layer  $< 18$  and a bottom layer within the polyhaline/seawater ranges, was found in the first four boxes (0–5.6 km) in spring and summer, whereas in fall and winter the vertical discontinuity was confined to the first two boxes within the lower estuary. As expected, vertical stratification was also observed during the spring tide survey.

In the stratified section of the estuary, the fluxes of chlorophyll *a* were always negative in the lower layer boxes (Figure 5), i.e., the consumption/loss of chlorophyll *a* surpassed production. On the other hand, chlorophyll *a* production was found in the upper boxes reaching  $2.118 \text{ mg m}^{-3} \text{ h}^{-1}$  (Figure 5E, Box 2A) during spring tide survey performed during the summer. For the ebb tide surveys, chlorophyll *a* production was associated with the lower salinity upper layers, regardless of the seasons, reaching a maximum value of  $2.750 \text{ mg m}^{-3} \text{ h}^{-1}$  (Figure 5B, Box 3A) during spring. In the winter and fall, Box 2A showed the higher chlorophyll *a* production within the estuary, with  $0.109 \text{ mg m}^{-3} \text{ h}^{-1}$  and  $0.274 \text{ mg m}^{-3} \text{ h}^{-1}$ , respectively. In stratified conditions, upper layer fluxes were always positive, showing a net biomass growth.

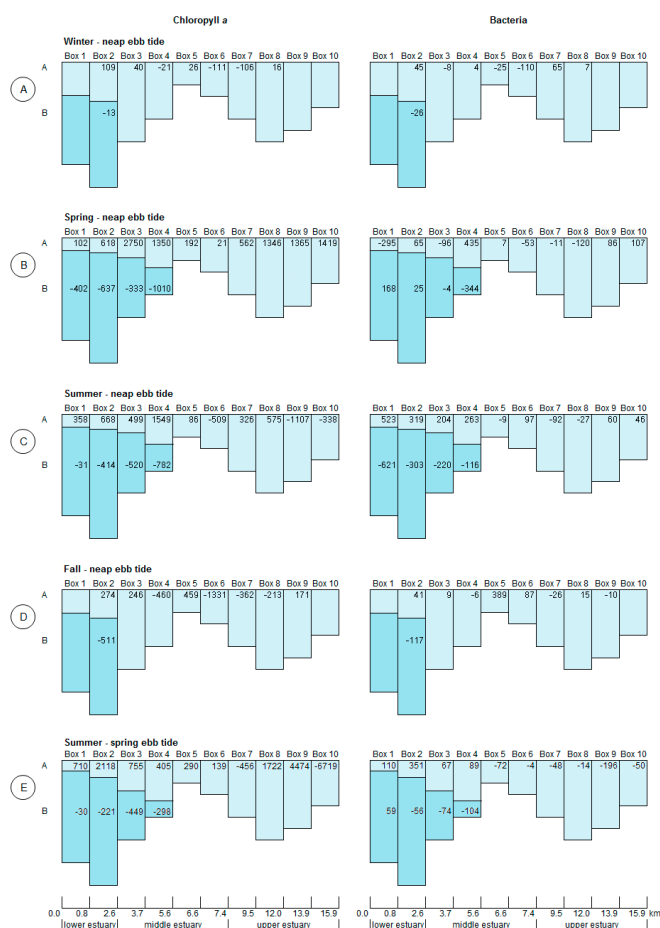


**Figure 5.** Model box results for chlorophyll *a* ( $10^{-3} \text{ mg m}^{-3} \text{ h}^{-1}$ ) and bacteria ( $10^9 \text{ cells m}^{-3} \text{ h}^{-1}$ ), rates of production (positive values) and loss (negative values) for the seasonal neap tides (A–D), and the summer spring tide (E). A—upper layer corresponding to salinity lower than 18 and B—lower layer corresponding to salinity higher than 18. The vertical axis represents the relative depth of each box.

A similar behavior was observed for bacterial fluxes. Bacteria removal processes were usually dominant within polyhaline/seawater boxes. However, the positive fluxes in the box 1B during spring neap tide and summer spring tide, suggested a possible seawater input of bacteria into the estuary on these occasions. With the exception of winter, the lower layer of the stratified zone showed the highest bacteria removal, a process boosted in summer ( $6.21 \times 10^{11}$  cells  $m^{-3} h^{-1}$ ; Figure 5C, Box 1B). Regarding the upper layer boxes, bacterial fluxes were positive, except in Boxes 1A and 3A ( $2.9 \times 10^{11}$  cells  $m^{-3} h^{-1}$  and  $9.6 \times 10^{10}$  cells  $m^{-3} h^{-1}$ , respectively) during spring neap tide, indicating biomass growth or production downstream, in accordance with chlorophyll *a*.

In most of the middle and in the upper estuary, salinities were always lower than 18, translating into a single layer box model. At this section of the estuary, fluxes of chlorophyll *a* fluctuated between positive and negative, with exception of the seasonal spring survey when production was observed throughout (Figure 5B, Boxes 3–10, and Figure S1). The highest chlorophyll *a* production occurred during the warmer months as expected. With the exception of the summer surveys, the river water seemed to be a source of chlorophyll *a* biomass, since the upstream boxes (corresponding to freshwater) had positive fluxes for chlorophyll *a*. Production of chlorophyll *a* was also present in the middle estuary. The comparison of the box models obtained for the two summer tidal surveys suggested a slight spatial dislocation of the boxes toward upstream, i.e., the box (n) in the neap tide seemed to be placed at the box (n + 1) of the spring tide, especially in the upper estuary. The higher chlorophyll *a* production reached  $4.474$  mg  $m^{-3} h^{-1}$  (Box 9, Figure 5E) during the spring tide. In regards to consumption, the higher values were  $1.107$  mg  $m^{-3} h^{-1}$  (Box 9, Figure 5C), and  $6.719$  mg  $m^{-3} h^{-1}$  (Box 10, Figure 5E), for neap and spring tides, respectively.

The bacterial behavior within the non-stratified stretch of estuary was also irregular, although freshwater appeared to introduce bacteria into the estuary as in the case of chlorophyll *a*, with exception of the fall. The highest bacterial removal was found in winter (Figure 5A, Box 6,  $1.10 \times 10^{11}$  cells  $m^{-3} h^{-1}$ ), and highest bacterial growth in the fall (Figure 5D, Box 5,  $3.89 \times 10^{11}$  cells  $m^{-3} h^{-1}$ ), within the middle estuary. Surprisingly, during the summer spring tide, all bacterial fluxes were negative, denoting the dominance of removal processes.

During the warmest months of the year, bacteria grew faster (Table 2), with higher values within the low and middle estuarine stretches, during the neap tide surveys, meaning that the population had the ability to potentially double several times over a single tidal cycle (12 h). On the other hand, the higher generation times were found during the coldest months.

**Table 2.** Bacteria generation times, calculated for boxes with growth, assuming the linearity of growth over 24 h.

		Generation Time (h)				
		Winter	Spring	Summer		Fall
Estuary Stretch	Box	Neap Tide	Neap Tide	Neap Tide	Spring Tide	Neap Tide
Lower estuary	box 1A	-	-	1.55	12.32	-
	box 1B	-	2.82	-	22.13	-
	box 2A	6.95	5.97	3.48	4.56	10.16
	box 2B	-	16.52	-	-	-
Middle estuary	box 3	-	-	-	-	53.56
	box 3A	-	-	6.81	27.43	-
	Box 4	101	-	-	-	-
	box 4A	-	2.01	5.90	22.40	-
	box 5	-	211	-	-	1.80
	box 6	-	-	16.47	-	11.23
Upper estuary	box 7	6.19	-	-	-	-
	Box 8	64.55	-	-	-	64.29
	box 9	-	10.40	17.41	-	-
	box 10	-	10.80	24.86	-	-

## 4. Discussion

### 4.1. Freshwater Inflow

The freshwater inflow was a major driving force for water circulation in the Lima estuary, coming essentially from the discharges of upstream dams, as reported for other temperate estuaries (e.g., [33]). Therefore, the inflow together with salinity was used to calculate the required coefficients for the box model. A remarked seasonality occurred with the highest values occurring in winter and the lowest in summer. When the discharge decreased, vertical stratification of the water column was established and the tidal influence dominated. This phenomenon occurred due to two major factors: the tidal forces were insufficient to overcome stratification, and the runoff did not eliminate the salt wedge resulting from the previous flood tide.

### 4.2. Chlorophyll *a* and Bacteria Dynamics

Chlorophyll *a* values measured in the Lima estuary (0.96–17.04 mg m<sup>-3</sup>) were within the range found in other temperate systems [34–36]. During the spring and summer seasons, chlorophyll *a* concentrations were substantially higher than during the winter and fall (Table 1). Several factors may explain the seasonal increasing of values, namely higher temperatures [37,38], greater light availability [37–40], and hydrodynamic conditions favorable to the existence of stratification/stabilization of water column, and longer water residence times [40].

In the spring and summer seasons, independently of the tide, chlorophyll *a* peaked in the upstream oligohaline area of the estuary (salinity 0.5–5), whereas in the fall it peaked in freshwater, and during winter in the downstream polyhaline area. The observed patterns during the warmest period of the year at the interface between freshwater and saltwater, were also reported previously [13], as well as for the fall [41]. Moreover, chlorophyll *a* peaks may also occur in higher salinity areas [40,42]. Chlorophyll *a* peaks spatially when growth rates increase and/or loss rates decrease. The latter include retention mechanisms, since the entrainment of exogenous chlorophyll *a* foment their accumulation, even in low growth rates [41]. With the exception of winter, the upper part of the estuary, surrounded by intensive agriculture (irrigated maize), seemed to behave as a source of chlorophyll *a*, as well as of nitrogen in the water column (Tables S1–S3). The same pattern was found in other estuaries [5,43]. During winter, chlorophyll *a* showed its maximum within the estuarine area with the highest suspended solids (Figure S1), and retention has been suggested as a mechanism to explain the abundance in less light availability locations [41], as in this case.

Bacterial concentrations (5.38–6.26 log<sub>10</sub> cells mL<sup>-1</sup>) were also similar to levels found in other temperate estuaries [4,44]. Bacterial abundance followed the expected seasonal pattern, with higher values in summer and spring, and minima in winter and fall [45]. The distribution of microorganisms within an estuary depends of the interaction of various dynamic processes, namely, growth, mortality, predation, and physical dispersion [20]. For estuaries with stratified waters, the variation in the hydrodynamic conditions can lead to important consequences in the control of the structure of microbial community and its activity. Salinity is one of the estuarine properties that can have relevance in the control of the communities arriving with the inflow of river water. This evidence appears to control the microbial abundance as a consequence of the dilution and “bactericidal” activity of salinity [46,47] in the polyhaline/euhaline range, and in the increased survival in the mesohaline salinity range [48]. Moreover, salinity not only controls the abundance [49] and activity of microorganisms, but also its community structure [50,51]. Previous studies suggested that salinity was determinant for bacterial communities, and seasonal changes in bacterial communities in both marine and brackish environments [52]. In this study, the behavioral trend presented by the chlorophyll *a* and bacteria within the estuarine salinity range and seasons was variable (Figure 4). Therefore, in this partially stratified system, the knowledge of the relationship between these variables and the salinity is insufficient to understand their behavior per se.

Along the estuary, bacteria presented two different behavioral trends, one for the warmest period of the year (spring and summer) and another for the coldest seasons (Figure 4). Although, the microbial

amount did not always decrease toward downstream, as reported in previous studies (e.g., [20]), during fall and winter the highest values were indeed found in the freshwater stretch. During spring and summer, increased bacterial cell counts were observed in the middle estuary, a mesohaline area in agreement with Ducklow et al. [53], in an intermediate zone of the estuary dominated by saltmarsh islands and shallow channels. The accretion of dissolved organic carbon and/or bacterial biomass from terrestrial inflow might help to explain the observed pattern [17]. Since in the Lima estuary a vertical stratification is always present (although varying in extent) in the downstream stretch, limited fluxes of advection and convection of microorganisms and substrate between the upper and lower layers may occur. Therefore, the substrate supply for bacteria and chlorophyll *a*, including light, can become priority factors in the stratified waters, due to nutrient reduction and light unavailability [4].

#### 4.3. Box Model Approach

Here, we constructed a box model based on the conservative properties of salinity and river flow to better understand the processes controlling the chlorophyll *a* and bacteria distribution in the estuary. This model is a simple and straightforward tool (does not require complex calculations and computer power), it is easy to apply and interpret, being therefore accessible for non-scientific end-users (e.g., managers). Moreover, since its development by Pritchard [7], it has been successfully applied to other estuaries (e.g., [4,20,54]). However, the simplification of a complex system implies some compromises in processes related with phytoplankton (e.g., primary production, predation, mortality), and bacteria (e.g., lateral inputs due to wastewater, death or predation). Therefore, it must be applied with caution.

For all surveys, according to the model (Figure 5), the sea end-member did not act as a source of chlorophyll *a*, given that the fluxes were always negative for salinities higher than 18. Indeed, chlorophyll *a* values were overall lower in higher salinities (Figure 4). In general, the bacterial fluxes for salinity above 18 were also negative, probably due to the dominance of some physical control, such as sedimentation, in the lower end of the estuary. In the summer neap tide, the loss of bacteria in the lower boxes was more pronounced in the lower estuary, while in the following spring tide, the trend was inverse, with a positive flux in box 1B. This trend was mimicked during the neap tide of the spring season when net bacterial growth occurred. Therefore, with the exception of the spring neap and summer spring tidal surveys, coastal waters did not appear to be a source of bacteria to the Lima estuary.

As a general picture, the upper limit of polyhaline/seawater appeared to regulate the coupling of chlorophyll *a* and bacteria regardless of the tide. Indeed, similar trends were found for chlorophyll *a* and bacterial fluxes in the lower, and part of the middle, estuary; with net growth (positive values) in the upper boxes and consumption (negative values) in the bottom boxes found.

Neap tide chlorophyll *a* production fluxes presented in both mesohaline and freshwater zones were higher in spring compared to summer, as reported for other estuaries [55,56]. In the middle estuary, the spring higher chlorophyll *a* production, despite higher solar radiation in the summer, can be explained by the greater availability of nutrients brought by winter mixing [56]. Comparing the summer spring/neap tides chlorophyll *a* behavior, a similar spatial trend was found, peaking in the mesohaline as well as in the low salinity uppermost stretch. The larger tidal amplitude during the spring tide event favored the availability of nutrients due to the potential increase of mixing, flooding, and further washout of tidal flats and saltmarshes within the estuary. Some authors (e.g., [57]) also noted a dichotomy between neap-spring tides.

During fall and winter, the chlorophyll *a* production peaked in the upper boxes of the lower estuary, corresponding to a higher temperature stretch (Figure S1), and higher river flow pushing the bloom toward sea end-member [40]. Nevertheless, the positive fluxes were rather modest when compared to the warmest period of the year.

The seasonal bacteria production during neap tides occurred usually in the upper layer boxes when stratification was present (positive fluxes), except for the two down-most boxes during spring.

Stratification, both vertical and horizontal, appeared to foster the co-existence of two bacterial populations during the warmest months, one associated to higher salinity, and another adapted to salinity below 10. Freshwater seemed to be a source of bacteria except in the fall, since bacterial growth was noticed in the uppermost boxes. Indeed, freshwater inflow plays a key role in the delivery of organic matter and nutrients to estuaries [17,58], acting as a carrier for chlorophyll *a* and bacteria. For salinities higher than 18, bacterial fluxes were negative. The resuspension of particles with the saline intrusion, followed by sedimentation in the slack tide period, could trap bacteria in sediments [59].

During the summer neap tide, bacteria growth was higher in the lower stretches, with fast generation times, increasing monotonically toward the upper part of the estuary (Table 2). A similar trend was found during the following spring tide, but generation times were higher, probably as a result of the synergistic interaction between freshwater and tidal flushing [60]. During the neap tide, the utilization of terrestrial dissolved organic carbon in the upper reaches of the estuary [53] may have played a pivotal role, as well as the higher values of total suspended solids (Figure S1), resulting in a larger amount of available, particle-attached bacteria [61] that grow faster than free-living bacteria [50]. Given that generation times are much lower than residence time of ca. seven days for the Lima estuary [3], an estuarine community can develop in intermediate salinities in addition to the presence of freshwater and marine populations [62].

Except for winter, bacteria growth peaked into estuary mid-stretch, as observed in Chesapeake Bay and in the Delaware estuary [53], in an area of the estuary with saltmarsh islands and shallow channels containing high concentrations of particulate matter, which can provide substrates for microbial colonization and growth [61]. The maximum growth of bacteria in the freshwater verified during the winter, may be related to a greater riverine nutrients input due to the increase of the river flow. In agreement with other studies (e.g., [62]), the bacterial production presented a clear seasonal pattern, being higher in summer, lower in winter, and intermediate in spring and fall.

Positive values of chlorophyll *a* production were followed by bacterial growth (Figure 5) within the lower estuary, except during spring. Bacterial biomass and production often presented covariance with phytoplankton (primary production or chlorophyll *a*), as reported by Hoch and Kirchman [63]. However, the uncoupling of bacterial production to primary chlorophyll *a* production is not uncommon in estuaries, especially when allochthonous carbon inputs are high [17]. The organic nutrition improvement factor due to the phytoplankton could be annulled, either by the release of compounds with anti-bacterial activity [4,64], or by the competition for the same substrate resulting in an effective control of bacterial dynamics [38,49,65].

## 5. Conclusions

The maximum concentrations of chlorophyll *a* were found in the upper oligohaline area regardless of the tide for all seasons, except during the winter, when the peak moved to the downstream polyhaline area. A net loss of chlorophyll *a* was always found at salinities above 18. For all surveys, the higher bacterial amount was found in the middle estuary, an area with saltmarsh islands, but also in the upper estuary during the coldest period of the year. Freshwater appeared to be the main source of bacteria during neap tides, with the exception of fall, whereas coastal waters have assumed this role during the summer spring tide and for the fall neap tide. Bacterial growth was higher during the warmest months of the year, with faster generation times in the lower stretches, increasing monotonically toward the upper estuary, being the highest at the spring tide. The coupling between chlorophyll *a* and bacteria was spatially limited by water column stratification while, upstream, the plankton responded differently to environmental conditions. The results showed the coupling between estuarine hydrodynamics and bacterial dynamics, thus explaining the differences between chlorophyll *a* and bacteria behavior in estuaries with seasonal variability and noticeable neap and spring tides. A future approach should aim at understanding the spatial and temporal salt wedge structure as a result of tidal dynamics (flood and ebb tides), coupled with the influence of different inflow regimes (seasonality),

toward the evaluation of the response of the entire estuarine system to the geomorphologic and river discharge variations imposed by human activity.

**Supplementary Materials:** The following are available online at <http://www.mdpi.com/2073-4441/11/3/588/s1>, Figure S1: Longitudinal profiles of temperature and total suspended solids in the temperate Lima estuary, Table S1: Mean concentrations  $\pm$  SE for key environmental parameters measured at the surface of the sampling sites: Secchi disc (SD)—m (in bold-bottom depth); temperature— $^{\circ}$ C; salinity; dissolved oxygen (DO)—mg O<sub>2</sub> L<sup>-1</sup>; pH; NO<sub>3</sub><sup>-</sup>, NO<sub>2</sub><sup>-</sup>, NH<sub>4</sub><sup>+</sup>, PO<sub>4</sub><sup>3-</sup>, N:P, and Si— $\mu$ M; chlorophyll *a* (CHL *a*)—mg m<sup>-3</sup>; total cell counts (TCC)—log<sub>10</sub> cells mL<sup>-1</sup>. In brackets—minimum and maximum values, Table S2: Mean concentrations  $\pm$  SE for key environmental parameters measured at middle depth of the sampling sites: temperature— $^{\circ}$ C; salinity; dissolved oxygen (DO)—mg O<sub>2</sub> L<sup>-1</sup>; pH; NO<sub>3</sub><sup>-</sup>, NO<sub>2</sub><sup>-</sup>, NH<sub>4</sub><sup>+</sup>, PO<sub>4</sub><sup>3-</sup>, N:P, and Si— $\mu$ M; chlorophyll *a* (CHL *a*)—mg m<sup>-3</sup>; total cell counts (TCC)—log<sub>10</sub> cells mL<sup>-1</sup>. In brackets—minimum and maximum values, Table S3: Mean concentrations  $\pm$  SE for key environmental parameters measured near bottom of the sampling sites: temperature— $^{\circ}$ C; salinity; dissolved oxygen (DO)—mg O<sub>2</sub> L<sup>-1</sup>; pH; NO<sub>3</sub><sup>-</sup>, NO<sub>2</sub><sup>-</sup>, NH<sub>4</sub><sup>+</sup>, PO<sub>4</sub><sup>3-</sup>, N:P, and Si— $\mu$ M; chlorophyll *a* (CHL *a*)—mg m<sup>-3</sup>; total cell counts (TCC)—log<sub>10</sub> cells mL<sup>-1</sup>. In brackets—minimum and maximum values.

**Author Contributions:** É.F., C.T. and A.A.B. conceived, designed and performed the study, and wrote the paper.

**Funding:** This work was partially funded by the Project INNOVMAR (Reference NORTE-01-0145-FEDER-000035), Research Line INSEAFOD, supported by the Northern Portugal Regional Operational Programme (NORTE2020), through the European Regional Development Fund (ERDF), and by the Strategic Funding UID/Multi/04423/2013 through national funds provided by the Portuguese Science Foundation (FCT) and ERDF, in the framework of the program PT2020. C. Teixeira also acknowledges FCT for a postdoctoral grant (ref. SFRH/BPD/110730/2015) through POCH, cofounded by MCTES and the European Social Fund.

**Acknowledgments:** The authors would like to thank Ana Machado, Cláudia Mendes, and Eva Amorim for their participation in the field work, as well as Lurdes Lima for lab assistance.

**Conflicts of Interest:** The authors declare no conflict of interest.

## References

- Jickells, T.D.; Andrews, J.E.; Parkes, D.J.; Suratman, S.; Aziz, A.A.; Hee, Y.Y. Nutrient transport through estuaries: The importance of the estuarine geography. *Estuar. Coast. Shelf. Sci.* **2014**, *150*, 215–229. [[CrossRef](#)]
- Robson, B.J.; Bukaveckas, P.A.; Hamilton, D.P. Modelling and mass balance assessments of nutrient retention in a seasonally-flowing estuary (Swan River Estuary, Western Australia). *Estuar. Coast. Shelf. Sci.* **2008**, *76*, 282–292. [[CrossRef](#)]
- Saraiva, S.; Pina, E.P.; Martins, E.F.; Santos, E.M. Modelling the influence of nutrient loads on Portuguese estuaries. *Hydrobiologia* **2007**, *587*, 5–18. [[CrossRef](#)]
- Bordalo, A.A.; Vieira, M.E.C. Spatial variability of phytoplankton, bacteria and viruses in the mesotidal salt wedge Douro Estuary (Portugal). *Estuar. Coast. Shelf. Sci.* **2005**, *63*, 143–154. [[CrossRef](#)]
- Wolanski, E.; Elliott, M. *Estuarine Ecohydrology—An Introduction*, 2nd ed.; Elsevier: Amsterdam, The Netherlands, 2016; pp. 1–87. ISBN 978-0-444-63398-9.
- Dyer, K.R. *Estuaries. A Physical Introduction*, 2nd ed.; John Wiley and Sons: Chichester, UK, 1997; ISBN 978-0-471-97471-0.
- Pritchard, D.W. Dispersion and flushing of pollutants in estuaries. *Proc. Am. Soc. Civ. Eng. J. Hydraul. Div.* **1969**, *95*, 115–124.
- Libes, S.M. *Introduction to Marine Biogeochemistry*, 2nd ed.; Elsevier Inc.: New York, NY, USA, 2009; pp. 65–100. ISBN 978-0-12-088530-5.
- Cloern, J. Tidal stirring and phytoplankton bloom dynamics in an estuary. *J. Mar. Res.* **1991**, *49*, 203–221. [[CrossRef](#)]
- Calbet, A.; Landry, M.R. Phytoplankton growth, microzooplankton grazing, and carbon cycling in marine systems. *Limnol. Oceanogr.* **2004**, *49*, 51–57. [[CrossRef](#)]
- Cermeño, P.; Maranon, E.; Pérez, V.; Serret, P.; Fernández, E.; Castro, C. Phytoplankton size structure and primary production in a highly dynamic coastal ecosystem (Ría de Vigo, NW-Spain): Seasonal and shorttime scale variability. *Estuar. Coast. Shelf. Sci.* **2006**, *67*, 251–266. [[CrossRef](#)]
- Kimmerer, W.J. Effects of freshwater flow on abundance of estuarine organisms: Physical effects or trophic linkages? *Mar. Ecol. Progr. Ser.* **2002**, *243*, 39–55. [[CrossRef](#)]

13. Azhikodan, G.; Yokoyama, K. Spatio-temporal variability of phytoplankton (Chlorophyll-a) in relation to salinity, suspended sediment concentration, and light intensity in a macrotidal estuary. *Cont. Shelf Res.* **2016**, *126*, 15–26. [[CrossRef](#)]
14. Roegner, G. Hydrodynamic control of the supply of suspended chlorophyll a to infaunal estuarine bivalves. *Estuar. Coast. Shelf Sci.* **1998**, *47*, 369–384. [[CrossRef](#)]
15. Valdes-Weaver, L.M.; Piehler, M.F.; Pinckney, J.L.; Howe, K.E.; Rossignol, K.; Paerl, H.W. Long-term temporal and spatial trends in phytoplankton biomass and class-level taxonomic composition in the hydrologically variable Neuse-Pamlico estuarine continuum, North Carolina U.S.A. *Limnol. Oceanogr.* **2006**, *51*, 1410–1420. [[CrossRef](#)]
16. Chaudhuri, K.; Manna, S.; Sarma, K.S.; Naskar, P.; Bhattacharyya, S.; Bhattacharyya, M. Physicochemical and biological factors controlling water column metabolism in Sundarbans estuary, India. *Aquat. Biosyst.* **2012**, *8*, 1–16. [[CrossRef](#)] [[PubMed](#)]
17. Hitchcock, J.N.; Mitrovic, S.M. Highs and lows: The effect of differently sized freshwater inflows on estuarine carbon, nitrogen, phosphorus, bacteria and chlorophyll a dynamics. *Estuar. Coast. Shelf Sci.* **2015**, *156*, 71–82. [[CrossRef](#)]
18. Anderson, O.R. The role of heterotrophic microbial communities in estuarine C budgets and the biogeochemical C Cycle with implications for global warming: Research opportunities and challenges. *J. Eukaryot. Microbiol.* **2016**, *63*, 394–409. [[CrossRef](#)] [[PubMed](#)]
19. Attermeyer, K.; Tittel, J.; Allgaier, M.; Frindte, K.; Wurzbacher, C.; Hilt, S.; Kamjunke, N.; Kamjunke, H. Effects of light and autochthonous carbon additions on microbial turnover of allochthonous organic carbon and community composition. *Microb. Ecol.* **2015**, *69*, 361–371. [[CrossRef](#)] [[PubMed](#)]
20. Painchaud, J.; Lefavre, D.; Therriault, J.C. Bacterial dynamics in the upper St. Lawrence estuary. *Limnol. Oceanogr.* **1996**, *41*, 1610–1618. [[CrossRef](#)]
21. Mallin, M.A.; Williams, K.E.; Esham, E.C.; Lowe, R.P. Effect of human development on bacteriological water quality in coastal watersheds. *Ecol. Appl.* **2000**, *10*, 1047–1056. [[CrossRef](#)]
22. INAG—Instituto da Água. Questões Significativas da Gestão da Água—Região Hidrográfica do Minho e Lima. 2009. Available online: [http://dqa.inag.pt/dqa2002/port/p\\_dispos/QSigaPP/Questoes\\_Minho\\_Lima\\_30\\_01\\_2009.pdf](http://dqa.inag.pt/dqa2002/port/p_dispos/QSigaPP/Questoes_Minho_Lima_30_01_2009.pdf) (accessed on 16 December 2012).
23. Vale, L.M.; Dias, J.M. The effect of tidal regime and river flow on the hydrodynamics and salinity structure of the Lima Estuary: Use of a numerical model to assist on estuary classification. *J. Coast. Res. Spec. Issue* **2011**, *64*, 1604–1608.
24. Azevedo, I.; Ramos, S.; Mucha, A.P.; Bordalo, A.A. Applicability of ecological assessment tools for management decision-making: A case study from the Lima estuary (NW Portugal). *Ocean Coast. Manag.* **2013**, *72*, 54–63. [[CrossRef](#)]
25. Almeida, C.M.R.; Mucha, A.P.; Vasconcelos, M.T. Role of different salt marsh plants on metal retention in an urban estuary (Lima estuary, NW Portugal). *Estuar. Coast. Shelf Sci.* **2011**, *91*, 243–249. [[CrossRef](#)]
26. Parsons, T.R.; Maita, Y.; Lalli, C.M. *A Manual of Chemical and Biological Methods for Seawater Analysis*; Pergamon Press: Oxford, UK, 1984; 173p, ISBN 0-08-030288-2.
27. SCOR-UNESCO. Determination of Photosynthetic Pigments in Sea Water. In *Monographs on Oceanographic Methodology*; UNESCO, Ed.; UNESCO Press: Paris, France, 1966; Volume 1, pp. 10–69.
28. Porter, K.G.; Feig, Y.S. The use of DAPI for identifying and counting aquatic microflora. *Limnol. Oceanogr.* **1980**, *41*, 1610–1618.
29. Herschy, R.W. *Streamflow Measurement*, 2nd ed.; E & FN Spon: London, UK, 1995; pp. 5–13. ISBN 978-0-41-919490-3.
30. Venice System. Symposium on the classification of brackish waters, Venice, Italy, 8–14 April 1958. *Arch. Oceanogr. Limnol.* **1958**, *11*, 1–248. Available online: <https://aslopubs.onlinelibrary.wiley.com/doi/abs/10.4319/lo.1958.3.3.0346> (accessed on 16 December 2012).
31. European Union (EU). Directive 2000/60/EC of the European Parliament and of the Council of 23 October 2000 establishing a framework for community action in the field of water policy. *Off. J. Eur. Union* **2000**, *L327*, 1–72.
32. Robarts, R.D.; Zohary, T.; Waiserl, M.J.; Yacobi, Y.Z. Bacterial abundance, biomass, and production in relation to phytoplankton biomass in the Levantine basin of the southeastern Mediterranean Sea. *Mar. Ecol. Prog. Ser.* **1996**, *137*, 273–281. [[CrossRef](#)]

33. Hofmeister, R.; Flöser, G.; Schartau, M. Estuary-type circulation as a factor sustaining horizontal nutrient gradients in freshwater-influenced coastal systems. *Geo-Mar. Lett.* **2017**, *37*, 179–192. [[CrossRef](#)]
34. Iriarte, A.; Villate, F.; Uriarte, I.; Alberdi, L.; Intxausti, L. Dissolved oxygen in a temperate estuary: The influence of hydro-climatic factors and eutrophication at seasonal and inter-annual time scales. *Estuaries Coast.* **2015**, *38*, 1000–1015. [[CrossRef](#)]
35. Carbone, M.E.; Spetter, C.V.; Marcovecchio, J.E. Seasonal and spatial variability of macronutrients and Chlorophyll *a* based on GIS in the South American estuary (Bahía Blanca, Argentina). *Environ. Earth Sci.* **2016**, *75*, 1–13. [[CrossRef](#)]
36. Gonçalves, D.A.; Marques, S.C.; Primo, A.L.; Martinho, F.; Bordalo, M.; Pardal, M.A. Mesozooplankton biomass and copepod estimated production in a temperate estuary (Mondego estuary): Effects of processes operating at different timescales. *Zool. Stud.* **2015**, *54*, 57. [[CrossRef](#)]
37. Winder, M.; Cloern, J.E. The annual cycles of phytoplankton biomass. *Phil. Trans. R. Soc. B* **2010**, *365*, 3215–3226. [[CrossRef](#)] [[PubMed](#)]
38. Buchan, A.; LeCleir, G.R.; Gulvik, C.A.; González, J.M. Master recyclers: Features and functions of bacteria associated with phytoplankton blooms. *Nat. Rev. Microbiol.* **2014**, *12*, 686–698. [[CrossRef](#)] [[PubMed](#)]
39. Barrio, P.; Ganju, N.K.; Aretxabaleta, A.L.; Hayn, M.; García, A.; Howarth, R.W. Modeling future scenarios of light attenuation and potential seagrass success in a eutrophic estuary. *Estuar. Coast. Shelf Sci.* **2014**, *149*, 13–23. [[CrossRef](#)]
40. Lu, Z.; Gan, J. Controls of seasonal variability of phytoplankton blooms in the Pearl river estuary. *Deep Sea Res. Part II Top. Stud. Oceanogr.* **2015**, *17*, 86–96. [[CrossRef](#)]
41. Bukaveckas, P.A.; Barry, L.E.; Beckwith, M.J.; David, V.; Lederer, B. Factors determining the location of the chlorophyll maximum and the fate of algal production within the tidal freshwater James river. *Estuaries Coast.* **2011**, *34*, 569–582. [[CrossRef](#)]
42. Fisher, T.R.; Harding, L.W., Jr.; Stanley, D.W.; Ward, L.G. Phytoplankton, nutrients, and turbidity in the Chesapeake, Delaware, and Hudson estuaries. *Estuar. Coast. Shelf Sci.* **1988**, *27*, 61–93. [[CrossRef](#)]
43. Desmit, X.; Ruddick, K.; Lacroix, G. Salinity predicts the distribution of chlorophyll *a* spring peak in the southern North Sea continental waters. *J. Sea Res.* **2015**, *103*, 59–74. [[CrossRef](#)]
44. Selje, N.; Simon, M. Composition and dynamics of particle-associated and free-living bacterial communities in the Weser estuary, Germany. *Aquat. Microb. Ecol.* **2003**, *30*, 221–237. [[CrossRef](#)]
45. Bacelar-Nicolau, P.; Nicolau, L.B.; Marques, J.C.; Morgado, F.; Pastorinho, R.; Azeiteiro, U.M. Bacterioplankton dynamics in the Mondego estuary (Portugal). *Acta Oecol.* **2003**, *24*, S67–S75. [[CrossRef](#)]
46. Hobbie, J.E. A comparison of the ecology of planktonic bacteria in fresh and salt water. *Limnol. Oceanogr.* **1988**, *33*, 750–764.
47. Munro, P.M.; Gauthier, M.J.; Breittmayer, V.A.; Bonjiovanni, J. Influence of osmoregulation processes on starvation survival of *Escherichia coli* in seawater. *Appl. Env. Microbiol.* **1989**, *55*, 121–124.
48. Bordalo, A.A. Microbiological water quality in urban coastal beaches: The influence of water dynamics and optimization of the sampling strategy. *Water Res.* **2003**, *37*, 3233–3241. [[CrossRef](#)]
49. Bunse, C.; Bertos-Fortis, M.; Sassenhagen, I.; Sildever, S.; Sjöqvist, S.; Godhe, A.; Gross, S.; Kremp, A.; Lips, I.; Lundholm, N.; et al. Spatio-temporal interdependence of bacteria and phytoplankton during a Baltic Sea spring bloom. *Front. Microbiol.* **2016**, *7*, 517. [[CrossRef](#)] [[PubMed](#)]
50. Campbell, B.; Kirchman, D.L. Bacterial diversity, community structure and potential growth rates along an estuarine salinity gradient. *ISME J.* **2013**, *7*, 210–220. [[CrossRef](#)] [[PubMed](#)]
51. Xia, X.; Guo, W.; Liu, H. Dynamics of the bacterial and archaeal communities in the Northern South China Sea revealed by 454 pyrosequencing of the 16S rRNA gene. *Deep Sea Res. Part II Top. Stud. Oceanogr.* **2015**, *117*, 97–107. [[CrossRef](#)]
52. Herlemann, D.P.R.; Lundin, D.; Andersson, A.F.; Labrenz, M.; Jürgens, K. Phylogenetic signals of salinity and season in bacterial community composition across the salinity gradient of the Baltic Sea. *Front. Microbiol.* **2016**, *7*, 1883. [[CrossRef](#)]
53. Ducklow, H.W.; Schultz, G.; Raymond, P.; Bauer, J.; Shiah, F.K. Bacterial Dynamics in Large and Small Estuaries. In *Microbial Ecology of Estuaries, Proceedings of the 8th International Symposium on Microbial Ecology, Halifax, NS, Canada, 9–14 August 1998*; Bell, C.R., Brylinsky, M., Johnson-Green, P., Eds.; Atlantic Canada Society for Microbial Ecology: Halifax, NS, Canada, 1999; pp. 105–111.

54. Testa, J.M.; Kemp, W.M. Variability of biogeochemical processes and physical transport in a partially stratified estuary: A box-modelling analysis. *Mar. Ecol. Prog. Ser.* **2008**, *356*, 63–79. [[CrossRef](#)]
55. Lyngsgaard, M.M.; Markager, S.; Richardson, K.; Møller, E.F.; Jakobsen, H.H. How well does chlorophyll explain the seasonal variation in phytoplankton activity? *Estuaries Coast.* **2017**. [[CrossRef](#)]
56. Martinez, E.; Antoine, D.; D’Ortenzio, F.; Montégut, C.B. Phytoplankton spring and fall blooms in the North Atlantic in the 1980s and 2000s. *J. Geophys. Res.* **2011**, *116*, 1–11. [[CrossRef](#)]
57. Van Alstyne, K.L.; Nelson, T.A.; Ridgway, R.L. Environmental chemistry and chemical ecology of “green tide” seaweed blooms. *Integr. Comp. Biol.* **2015**, *55*, 518–532. [[CrossRef](#)]
58. Liu, W.C.; Chan, W.T. Assessment of climate change impacts on water quality in a tidal estuarine system using a three-dimensional model. *Water* **2016**, *8*, 60. [[CrossRef](#)]
59. Kara, E.; Shade, A. Temporal dynamics of south end tidal creek (Sapelo Island, Georgia) bacterial communities. *Appl. Environ. Microbiol.* **2009**, *75*, 1058–1064. [[CrossRef](#)] [[PubMed](#)]
60. Wan, Y.; Qiu, C.; Doering, P.; Ashton, M.; Sun, D.; Coley, T. Modeling residence time with a three-dimensional hydrodynamic model: Linkage with chlorophyll *a* in a subtropical estuary. *Ecol. Model.* **2013**, *268*, 93–102. [[CrossRef](#)]
61. Vallières, C.; Retamal, L.; Ramlal, P.; Osburn, C.L.; Vincent, W.F. Bacterial production and microbial food web structure in a large arctic river and the coastal Arctic Ocean. *J. Mar. Syst.* **2008**, *74*, 756–773. [[CrossRef](#)]
62. Crump, B.C.; Hopkinson, C.S.; Sogin, M.L.; Hobbie, J.E. Microbial biogeography along an estuarine salinity gradient: Combined influences of bacterial growth and residence time. *Appl. Environ. Microbiol.* **2004**, *70*, 1494–1505. [[CrossRef](#)]
63. Hoch, M.P.; Kirchman, D.L. Seasonal and inter-annual variability in bacterial production and biomass in a temperate estuary. *Mar. Ecol. Prog. Ser.* **1993**, *98*, 83–295. [[CrossRef](#)]
64. Hulot, F.D.; Morin, P.J.; Loreau, M. Interactions between algae and the microbial loop in experimental microcosms. *Oikos* **2001**, *95*, 231–238. [[CrossRef](#)]
65. Martinussen, I.; Thingstad, T.F. Utilization of N, P and organic C by heterotrophic bacteria. II. Comparison of experiments and a mathematical model. *Mar. Ecol. Prog. Ser.* **1987**, *37*, 285–293. [[CrossRef](#)]



© 2019 by the authors. Licensee MDPI, Basel, Switzerland. This article is an open access article distributed under the terms and conditions of the Creative Commons Attribution (CC BY) license (<http://creativecommons.org/licenses/by/4.0/>).